Title	Development of a Hip Joint Model for Finite Volume Simulations
Authors(s)	Cardiff, Philip, Karac, Aleksandar, FitzPatrick, David P., et al.
Publication date	2013-12-03
Publication information	Cardiff, Philip, Aleksandar Karac, David P. FitzPatrick, and et al. “Development of a Hip Joint Model for Finite Volume Simulations.” ASME International, December 3, 2013. https://doi.org/10.1115/1.4025776.
Publisher	ASME International
Item record/more information	http://hdl.handle.net/10197/5937
Publisher's statement	This is a preprint of an article published in Journal of Biomechanical Engineering, 136 (1), available at http://dx.doi.org/10.1115/1.4025776
Publisher's version (DOI)	10.1115/1.4025776

Development of a Hip Joint Model for Finite Volume Simulations

P.Cardiff[a,*], A.Karač[b], D.FitzPatrick[a], R.Flavin[a], A.Ivanković[a]

[a]*School of Mechanical and Materials Engineering, University College Dublin, Belfield, D4, Dublin, Ireland*
[b]*Faculty of Mechanical Engineering, University of Zenica, Fakultetska 1, 72000 Zenica, Bosnia and Herzegovina*

Abstract

This paper establishes a procedure for numerical analysis of hip joint using the Finite Volume method. Patient-specific hip joint geometry is segmented directly from computed tomography and magnetic resonance imaging datasets and the resulting bone surfaces are processed into a form suitable for volume meshing. A high resolution continuum tetrahedral mesh has been generated where a sandwich model approach is adopted; the bones are represented as a stiffer cortical shells surrounding more flexible cancellous cores. Cartilage is included as a uniform thickness extruded layer and the effect of layer thickness is investigated. To realistically position the bones, gait analysis has been performed giving the 3-D positions of the bones for the full gait cycle. Three phases of the gait cycle are examined using a Finite Volume based custom structural contact solver implemented in open-source software OpenFOAM.

Keywords: hip joint, gait analysis, bone segmentation, volume meshing,

---

[*] Corresponding author. *Tel.*: +353 1 716 1880
Email address: `philip.cardiff@ucd.ie` (P.Cardiff)

Preprint submitted to Journal of Biomechanical Engineering *May 4, 2013*

Finite Volume method, OpenFOAM, contact stress analysis

1. Introduction

During routine activities such as walking or stair climbing, the hip joint experiences complex loading scenarios determined by the musculotendon forces, inertia and gravity. As a consequence of the limitations of *in vivo* and *in vitro* hip joint studies, numerical models of the hip joint have increasingly been considered to better understand the mechanics of the joint. Potentially, these *in silico*[1] studies of the hip joint may provide an effective tool for analysis of hip joint mechanics and stability, helping orthopaedists make confident surgical decisions.

Numerical methods and computing power have progressed considerably since Brekelmans et al. [1] first developed a 2-D finite element model of the femur in the early seventies. In preference to model geometry derived from radiographs, recent realistic hip models are now typically captured directly from patient-specific computed tomography (CT) or magnetic resonance imaging (MRI) datasets [2–9]. The hip bones are commonly represented as *sandwich structures* consisting of two discrete types of bone [2, 3, 5]; a stiffer outer shell of cortical bone surrounding a more flexible inner core of cancellous bone. In more recent years, CT-based material property assignment has become more popular [10–13], where the stiffness of each finite element is assigned based on CT Hounsfield pixel intensities. This approach represents an improvement on the more traditional bi-material sandwich model

---

[1] The phrase *in silico*, coined in 1989 as an analogy to the Latin phrases *in vivo* and *in vitro*, is an expression meaning "performed on computer or via computer simulation".

approach, however, the exact empirical relationship between Hounsfield intensity and stiffness can be difficult to determine and verification is not trivial [11, 12].

Although models of the hip joint have progressed considerably, there are still a number of shortcomings. Due to computational limits, the mesh is often of insufficient resolution to capture the true anatomy, cortical bone is often represented by degenerative shell elements, and bone surface meshes can be over-smoothened to deal with the understandably complex task of volumetric meshing. In spite of the steady increase in mesh densities, recent models are still yet to approach the high resolution required to capture large local stress gradients present in the contacting regions, giving possible explanation of why hip contact pressure predictions of more recent studies are larger than older studies [2, 4, 5, 14].

Numerical analysis of hip joint mechanics may be performed using one of many approaches, however, due to its well established role in computational structural mechanics, finite element (FE) analysis is the most widely employed method [1, 3, 4, 14–20]. Nonetheless, the Finite Volume (FV) method, being attractively simple yet strongly conservative in nature, has become a viable alternative in many solid mechanics applications [21–39]. Accordingly, the current work employs a cell-centred FV structural contact procedure to numerically examine the hip joint, implemented in open-source `C++` based software OpenFOAM (Open Source Field Operation and Manipulation, version 1.6-ext) [40–42], where the implemented physics and numerical algorithms may be viewed and are open to academic scrutiny, which is not possible with *black box* commercial codes.

2. Methods

2.1. Geometry Generation

Extraction of the hip bone geometry from tomography images is not a trivial task and care must be taken to avoid the loss of significant geometrical information. This section establishes a procedure for the generation of faithful hip bone volume meshes from patient specific tomography image sets.

CT and MRI scans were acquired of the hip joint of a 23-year-old male subject with no congenital or acquired pathology. The CT images (512×512 pixels, $0.7422 \times 0.7422 \times 1.2500$ mm) and MRI images (256×256 pixels, $1.6797 \times 1.6797 \times 2.9999$ mm) spanning from mid femur to second lumbar vertebra were obtained using the GE medical systems LightSpeed VCT [45] and GE medical systems Signa HDxt [45] scanners, respectively.

Using an automated thresholding technique, implemented in open-source software 3DSlicer (version 4.0) [46], the cortical bone is extracted by selecting pixels in the range 400–1585 Hounsfield Units (HU), while the cancellous bone is extracted selecting pixels in the range 200–400 HU [47]. Subsequently, the exterior bone surfaces are clearly discernible, and with minimum user effort, manual separation of the femur, pelvis and sacrum is performed. However, the cortical-cancellous bone interface can be much more difficult to distinguish necessitating time consuming manual segmentation. During the difficult task of distinguishing the cortical-cancellous bone interface, the MRI image set can be combined with the CT images, using a *fast rigid registration* procedure [46], limiting the subjectively of the segmentation.

Once the bone pixels of interest have been selected, an enclosing triangulated surface is constructed using a marching cubes procedure [46], producing a castellated surface mesh of the bone[2], illustrated in Figure 1(a).

To remove unwanted noise, the castellated surface meshes are smoothed to 10 iterations using a volume conserving Laplacian smoothing algorithm (Figure 1(b)) [48], as implemented in the open-source software Meshlab [49].

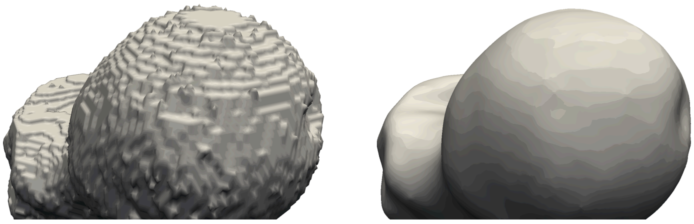

(a) Before (b) After

Figure 1: Volume Conservative Smoothing of the Bone Surfaces

Decimation, the process of combining small faces together, is conducted using a *quadric based edge collapse decimation* procedure, making the surface files more manageable for subsequent meshing procedures. A decimation factor of 0.2 is employed reducing the number of faces by a factor of five, with negligible effect to the bone features.This has been verified using open-source software Metro [50] by examining the geometric deviation between the original surface mesh and the decimated mesh. The mean geometric deviation is 0.0059 mm and the maximum is 0.1441 mm, which is considered acceptable.

---

[2] In this context, *castellated* refers to the resemblance of the mesh to the battlements on top of a medieval castle.

Finally, cleaning operations are performed on the surface mesh where close vertices are merged, short edges are removed, small holes are filled, and isolated faces and vertices are eliminated [51], and the final surfaces (Figure 2) are exported in stereolithography (STL) format - a facet based surface composed of triangles - suitable for input to most volumetric meshing software.

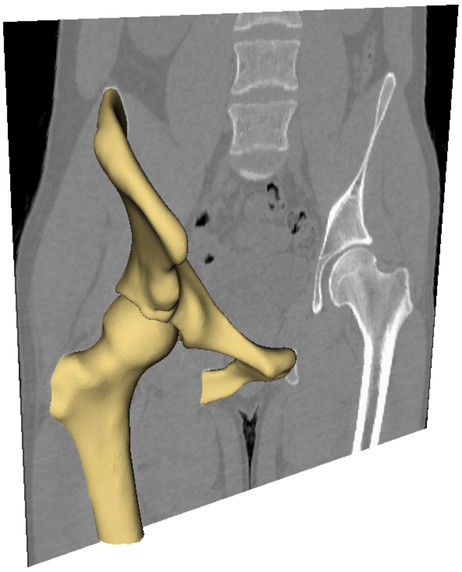

Figure 2: Final Processed Bone Exterior Surfaces Embedded in a Frontal CT Slice

2.2. Volume Meshing

Although, hexahedral meshes have been found more accurate than tetrahedral meshes [52, 53], generation of fully hexahedral hip joint meshes is far from a trivial process. Consequently, tetrahedral meshes are often employed, as is the case in the current study.

The femur, pelvis and cortical-cancellous STL surfaces are imported into ANSYS ICEM CFD [54], and partitioned into patches of interest - distal femur, femur head, acetabulum, iliosacral joint and pubic symphysis joint - for application of boundary conditions. The cortical and cancellous bone volumes are meshed using the patch independent Delaunay tetrahedral approach, and incrementally smoothed to improve the quality. Triangular prisms are *grown* from the boundary surface and cortical-cancellous interface, which is favourable for accurate boundary stresses, and the entire volume mesh is incrementally smoothed. The volume meshes are exported via the ANSYS Fluent ".msh" format and converted to the OpenFOAM format using the OpenFOAM utility `fluent3DMeshToFoam`.

To overcome inferior quality cells in thin cortical bone regions, smaller local cell sizes are required, and the minimum cortical bone thickness has been limited to 1.5 mm in troublesome areas.

To create the articular cartilage volume meshes, the femur and pelvis articular surface meshes are extruded in the surface normal direction by 0.6 mm using the OpenFOAM utility `extrudeMesh`. The cartilage thickness, t, has been determined using the approximate acetabulum radius, R_a, and the approximate femoral head radius, R_f [4]:

$$t = \frac{R_a - R_f}{2} \tag{1}$$

where $R_a = 27.6$ mm and $R_f = 26.4$ mm have been determined by manually fitting spheres.

The final high resolution hip joint volume mesh, containing a total of 569 418 cells (266 817 cortical, 253 316 cancellous, 49 285 cartilage), is shown in Figure 3. The average cell breadth on the articular surfaces is approximately

0.5 mm, ensuring good resolution of contact stress gradients. However, ultimately the geometric accuracy of the model is limited by the resolution of the tomography images.

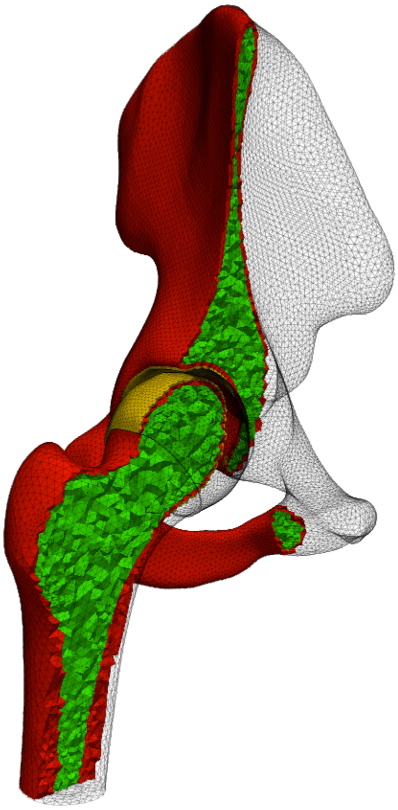

Figure 3: Hip Joint Model Material Distribution (Cortical Bone in Red, Cancellous Bone in Green and Cartilage in Yellow, Cells Removed for Visualisation)

2.3. Gait Analysis

Gait analysis, the systematic study of locomotion, has been performed on the subject from which the tomography images have been obtained, using the CODA (Codamotion V6.69H-CX1/MPX30) movement analysis system [55, 56]. The kinematic data of 3-D positions, measured at 200 Hz, has been analysed and processed using a custom written OpenFOAM utility `visualiseGaitData` [36, 43]. The *Visualisation Toolkit* (VTK) files generated by the `visualiseGaitData` utility allow visualisation of a *stick-man* representation of the gait cycle (Figure 4) in open-source software ParaView [58], enabling accurate determination of the beginning of each gait event.

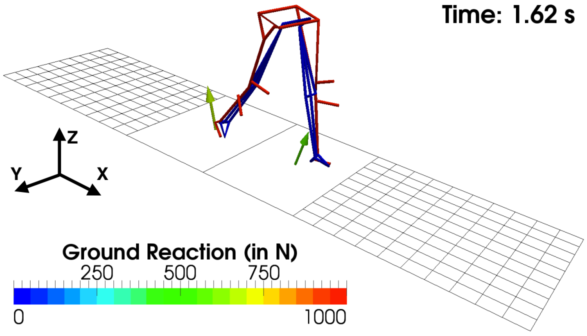

Figure 4: Gait Cycle Data Processed with `visualiseGaitData` Utility

A developed custom OpenFOAM utility `rotateRigidFemur` employs the kinematic gait data to calculate the time-varying position of the femur relative to the pelvis, allowing accurate positioning of the femur volume mesh relative to the pelvis for any phase of the gate cycle.

2.4. Finite Volume Structural Solver & Contact Procedure

A FV-based transient structural contact solver, `elasticContactNonLinULSolidFoam`, has been specifically developed to analyse the hip joint [36, 43, 59], with inertia and body forces being neglected in the current analyses. Here, linear elastic material properties are assumed and the updated

Lagrangian mathematical model is applied. Special attention is given to the contact algorithm, where a recently developed FV procedure based on the frictionless penalty method has been used [33]. Two potentially contacting surfaces are designated as the master and slave surfaces, and during the iterative procedure, the slave vertices are checked for penetration of the master surface. If a slave vertex does penetrate, an increment of interface force is applied between the slave vertex and the master surface.

The contact algorithm is controlled via three main parameters, namely, the interface stiffness, synonymous with the penalty factor or penalty stiffness, the gap tolerance and the contact correction frequency. The penalty factor controls the addition of interface force increments. Its choice affects the convergence of the contact procedure; if the penalty factor is too high then the contact may not converge, if too low the contact may take a prohibitively long time to converge. The gap tolerance specifies the extent of penetration. If the gap tolerance is too large, the bodies will penetrate by a large amount and the contact pressures will be underestimated. Conversely, if too small, the convergence of the contact procedure will be adversely affected. The contact correction frequency factor specifies how often the contact procedure is to be invoked during the inner iteration loop. It should be noted that as long as the procedure converges, the penalty factor and contact correction frequency do not affect the predicted mechanics, as an iterative procedure is employed ensuring the contact constraints are respected within the user defined gap tolerance.

3. Results

The hip joint is numerically analysed at three different phases of the gait cycle, namely:

- The **mid-stance** phase;
- The hip force peak following the **heel-strike** phase;
- The hip force peak prior to the **toe-off** phase.

3.1. Hip Joint Model Setup

The three hip joint models are shown in Figure 5. All materials are represented as hypoelastic, homogenous and isotropic and the material distribution is displayed previously in Figure 3. The cortical bone is assigned a Young's modulus of 17 GPa and a Poisson's ratio of 0.3 [2, 4–7, 14, 60–63], the cancellous bone is assigned a Young's modulus of 800 MPa and a Poisson's ratio of 0.2 [63, 64], and the articular cartilage is assigned a Young's modulus of 12 MPa and a Poisson's ratio of 0.45 [19, 65].

As boundary conditions, shown graphically in Figure 6, the pelvis is fixed at the iliosacral and pubic symphysis joints, and the distal femur is displaced in the femur axial direction into the acetabulum such that resulting total hip joint force is as measured *in vivo* by Bergmann et al. [44]. At *mid-stance* and *toe-off*, the hip joint force is twice body weight, 1 611 N, in the femur axial direction. For the *heel-strike* model, the femur axial force is 1 917 N, equivalent to 2.38 times body weight.

The remaining femur and pelvis surfaces are specified as traction-free. Custom boundary conditions with non-orthogonal corrections, previously described [36, 59], are employed and the gradient terms are calculated using

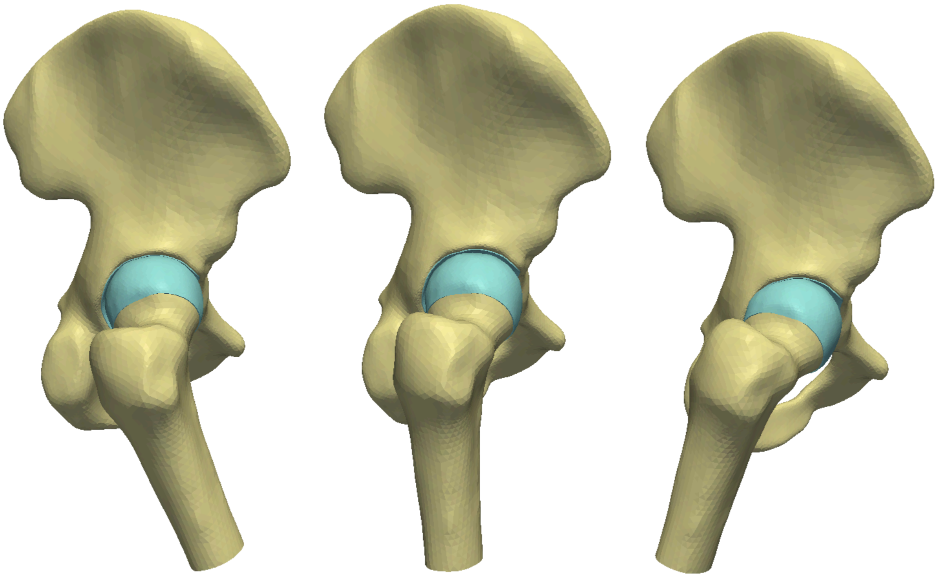

(a) *Heel-Strike* (b) *Mid-Stance* (c) *Toe-Off*

Figure 5: Hip Joint Models

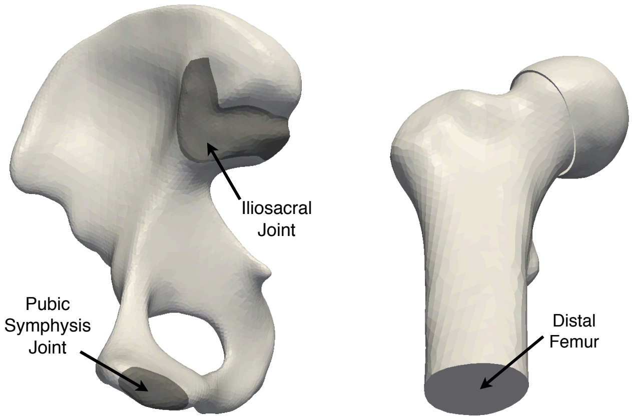

(a) Fixed Iliosacral & Pubic Symphysis Joints (b) Displaced Distal Femur

Figure 6: Boundary Conditions

the least squares method[3]. The models are solved in one load increment and inertia and gravity forces are neglected.

For the contact procedure, the pelvis articular cartilage surface is designated as the master and the femur articular surface as the slave. The contact penetration distances have been calculated using the *contact-spheres* approach [35]. A contact gap tolerance of 9×10^{-6} m is employed, the penalty factor is 6×10^8 and the contact correction frequency is 40.

3.2. Solution Process

The linear system formed by the discretisation of the momentum equation is iteratively solved using a geometric multi-grid[4] [66] segregated approach, where each of the three components of momentum equation are separately solved in terms of displacement increment. The final solution tolerance is set to 10^{-7}. An additional *relative* residual, defined as the maximum difference between successive displacements field solutions [36], must also reach the prescribed tolerance.

The models have been solved in parallel on a distributed memory supercomputer using 32 CPU cores (Intel Xeon E5430 Quad Core 2.66 GHz) in an approximate clock time of 10 hours.

Figure 7(a) displays the solution convergence for a typical model, showing that both the solver residual and the relative residual reach the predefined tolerance of 10^{-7} in approximately 160 000 outer iterations. Although a rel-

---

[3] The OpenFOAM `extendedLeastSquares` gradient scheme is employed as it assumes non-orthogonal boundary cells, unlike the `leastSquares` gradient scheme.

[4] The OpenFOAM GAMG linear solver has been employed, where the coarsest solution grid is set to the square-root of the average number of cells on each processor.

atively aggressive under-relaxation factor of 0.05 has been applied to achieve convergence, high frequency oscillations are still visible in the residuals most likely due to the nonlinear nature of the contact as well as lower quality cells. Figure 7(b) shows the convergence of the contact penetration to the predefined gap tolerance 9×10^{-6} m, where it can be seen that the contact converges at approximately 60 000 outer iterations and the remaining outer iterations are required to converge the displacements increments.

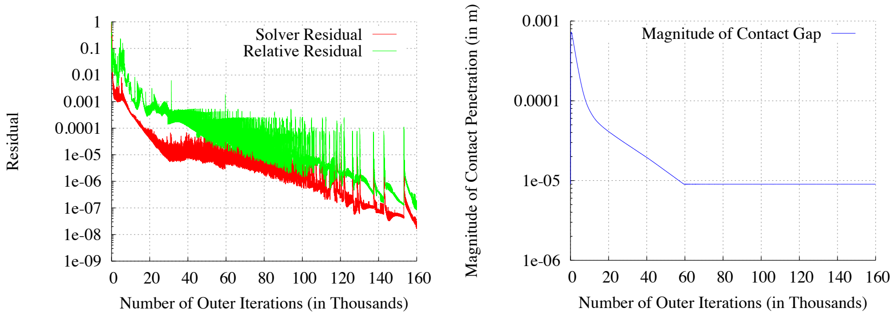

Figure 7: Typical Model Solution Convergence

The collection of softwares employed in the current work is summarised in Appendix A.

3.3. Contact Stress Analysis

The von Mises stress distribution of the *mid-stance* model is shown in Figure 8. The most highly stressed areas, of 30 to 50 MPa, are found in the ilium directly above the acetabulum, the acetabular roof bone as well as near the fixed iliosacral joint. The scale of Figure 8 ranges from 0 to 10 MPa to allow clearer viewing of the highly stressed regions.

Examining the contact pressure distribution, shown in Figure 8(a), three distinct contact regions are discernible, occurring in anterior superior, pos-

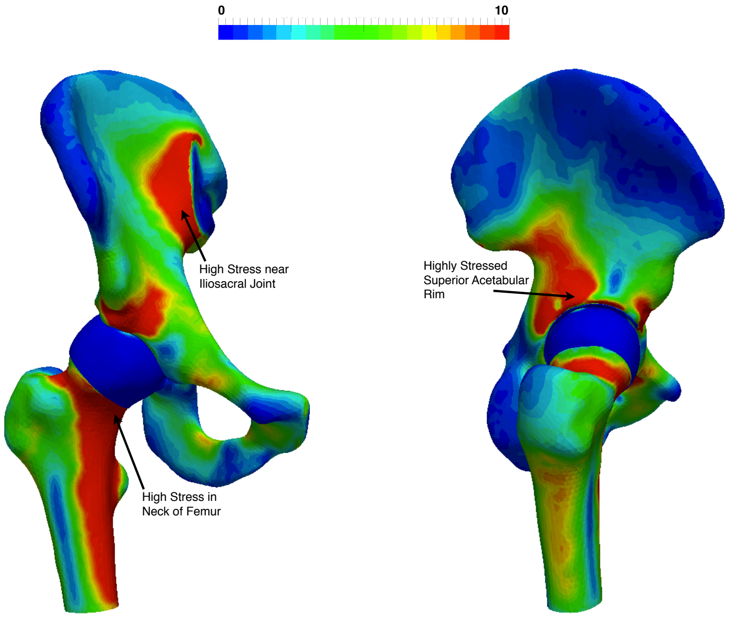

High Stress near Iliosacral Joint

High Stress in Neck of Femur

Highly Stressed Superior Acetabular Rim

(a) Anterior View Von Mises Stress (in MPa)

(b) Lateral View Von Mises Stress (in MPa)

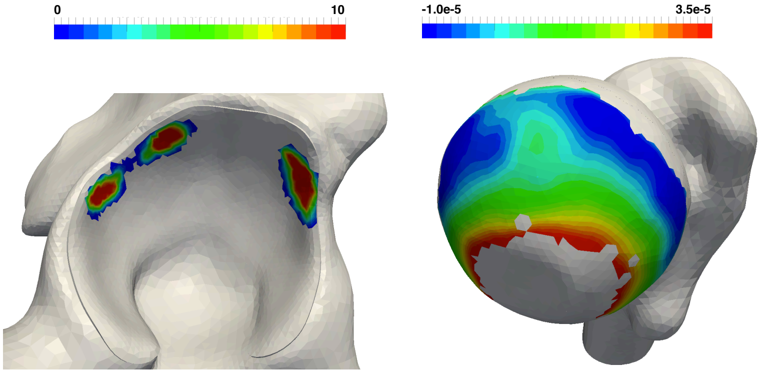

(a) Contact Pressure (in MPa)

(b) Contact Gap (in m)

Figure 8: *Mid-Stance* Model

terior superior and superior regions of the acetabulum. The maximum predicted contact pressure is 26 MPa occurring in the most superior contact region. The predicted contact area is 3.96×10^{-4} m^2 and has been calculated by summing the articular surface faces with a pressure greater than 1 kPa. The average contact pressure is 6.28 MPa and has been calculated by dividing the total contact normal force by the contact area. The total contact normal force, C_n, is calculated by:

$$C_n = \sum_f \frac{\mathbf{\Gamma}_f}{|\mathbf{\Gamma}_f|} \cdot (\mathbf{\Gamma}_f \cdot \boldsymbol{\sigma}_f) \tag{2}$$

where $\sum_f$ refers to the summation over all the faces of the articular surface and $\mathbf{\Gamma}_f$ is the face area vector.

Inspecting the model contact gap, as shown in Figure 8(b), the anterior superior and posterior superior regions show the most negative contact gap, relative to the superior region of the femoral head.

When the von Mises stress distribution of the *toe-off* and *heel-strike* models are examined, the most highly stressed areas occur in the bone superior and posterior to the acetabulum. As with the *mid-stance* model, the acetabular roof is highly stressed, in particular directly above the contact regions. Additionally, the bone around the iliosacral joint experiences high stresses.

Inspecting the contact regions of the *toe-off* and *heel-strike* models, shown side-by-side in Figures 9, distinct contact areas are once again visible. As with the *mid-stance* model, three contact regions occur in the *heel-strike* model, where the maximum predicted contact pressure is 26 MPa, the contact area is 3.83×10^{-4} m^2 and the average pressure is 10.1 MPa. In contrast, two contact regions occur in the *toe-off* model, where the maximum predicted contact pressure is 23 MPa, the contact area is 4.62×10^{-4} m^2 and the average pressure is 5.93 MPa.

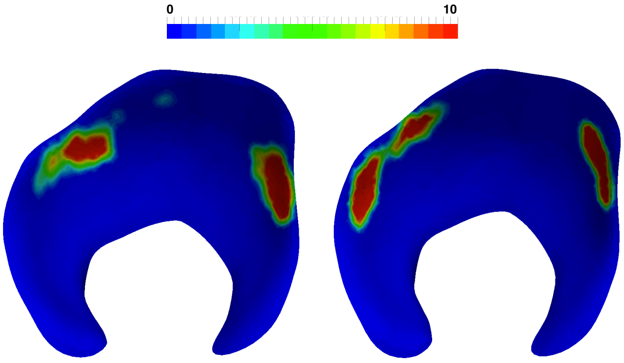

(a) *Toe-Off* (b) *Heel-Strike*

Figure 9: Contact Pressures of the *Toe-Off* & *Heel-Strike* Models (in MPa)

To ensure the predicted results are mesh independent, an additional *mid-stance* simulation has been performed using a more dense globally refined mesh. The refined mesh, containing a total of 769 529 cells (25% more cells than the original mesh) with an average articular surface cell breadth of approximately 0.42 mm, predicted a maximum contact pressure of 26.67 MPa, which is within 3% of the original mesh predictions, and stress distributions close to the original mesh, demonstrating mesh independence.

3.4. Effect of Cartilage Thickness

As the current models have approximated the articular cartilage as a 0.6 mm constant thickness layer, two additional simulations of *mid-stance* have been performed with increased cartilage thickness by 20% to 0.72 mm, and decreased thickness by 20% to 0.48 mm.

For the thinner cartilage model (0.48 mm), the maximum contact pressure is 34.58 MPa, the average contact pressure is 9.30 MPa, and the contact area is 2.51×10^{-4} m^2. For the thicker cartilage model (0.72 mm), the maximum predicted contact pressure is 21.59 MPa, the average contact pressure is 6.86 MPa, and the contact area is 3.59×10^{-4} m^2. Table 1 summarises the results for the three distinct cartilage thicknesses.

Cartilage Thickness (in mm)	Maximum Pressure (in MPa)	Average Pressure (in MPa)	Area (in m^2)
0.48	34.58	9.30	2.50×10^{-4}
0.60	26	6.28	3.96×10^{-4}
0.72	21.59	6.86	3.59×10^{-4}

Table 1: Effect of Cartilage Thickness on the Contact Mechanics of the *Mid-Stance* Model

4. Discussion

Inspecting the regions of greatest stress in the *mid-stance* model, the pelvis is relatively highly stressed in the acetabular roof, the ilium above the acetabulum and at the iliosacral joint. On closer analysis of the femur, the body of the femur holds much of the stress where significant bending occurs. These predictions agree well with results from numerical models in literature [2, 4, 14, 16, 19, 61, 63, 67], and it has been noted the large predicted stresses in the vicinity of the iliosacral joint are contributed to by the rigid fixture boundary condition [68].

Examining the predicted contact pressure distributions, the analyses suggest that the hip joint contact is not perfectly congruent and that there are distinct regions of local high contact pressure, agreeing with previous FE predictions [4, 14]. Comparing the contact mechanics of the *mid-stance* model with values from literature, the predicted contact pressures are larger than the reported values. Peak contact pressures in literature vary from 1 to 18 MPa [2, 4, 14, 16, 19, 61, 63, 67], whereas the maximum predicted contact pressure in the *mid-stance* model is 26 MPa. A possible explanation for this difference may be attributed to the simplifying assumptions commonly made in literature with regard to spherical congruent contact surfaces that overestimate contact areas, hence underestimating contact pressures. Additionally, many of the published numerical models represent the contact surfaces with relatively low resolution grids essentially averaging local contact stress peaks. A contributing factor that may result in the current model overestimating the contact pressure may be ascribed to simplifying assumptions with regard to the uniform bone mechanical properties and the constant thickness articular cartilage. Employing a stiffness of 17 GPa for the acetabular cortical bone may overestimate the stiffness of the pelvis, reducing the natural congruency of the joint and increasing contact stresses. A more realistic representation of varying cartilage thickness in addition to spatially varying tomography-based bone properties would certainly result in a more faithful model.

Analysing the effect of cartilage thickness has shown a considerable influence on the predicted mechanics. As expected, it has been found that there is an inverse relationship between the cartilage thickness and maximum contact pressure, where the maximum contact pressure increases by approximately 60% as the cartilage thickness decreases by 33% from 0.72 to 0.48 mm. However, surprisingly at first, the middle thickness (0.6 mm) model predicts the lowest average contact pressure. The reason for this may be deciphered by noticing that the contact pressure increases in the thicker cartilage model in the anterior and posterior regions of the acetabulum and lowers in the superior region. In reality, it is expected that the physiological cartilage thickness is greater on the superior femur head surface, therefore increasing the overall cartilage thickness may overestimate the thickness in the anterior and posterior regions of the acetabulum and femur head.

Of the three phases of gait examined, as anticipated the largest stresses and contact pressures occur in the *heel-strike* model, corresponding to the peak in gait cycle total joint forces. For all models, the predicted stress values and locations are consistent with previous FE studies [2, 4, 14, 16, 19, 36, 61, 63, 67], however, the magnitude of maximum contact pressures are greater than previously predicted. The effect of cartilage thickness has been examined and as expected the maximum predicted contact pressure has been found to be inversely related to the cartilage thickness, with the case of the thinnest cartilage producing the greatest maximum contact pressure. However, the largest average contact pressure has been found in the thickest cartilage case, most likely due to the assumption of constant thickness cartilage resulting in underestimation of superior cartilage thickness and overestimation of anterior/posterior cartilage thickness.

All presented results show that this novel numerical model, based on Finite Volume Method as implemented in an open-source software, represent a powerful alternative to well-established commercial FE-based softwares.

As its object-oriented nature permits complex custom routines to be implemented in an efficient manner, further improvement of the current model will be focused on implementation of material properties based on CT Hounsfield pixel intensities and on employment of physiologically realistic musculotendon loading models [36, 43].

5. Conflict of Interest Statement

There is no conflict of interest.

6. Acknowledgements

Financial support from TEKNO Surgical Ltd. is gratefully acknowledged. The authors thank Mike Walsh and Damien Kiernan of the Central Remedial Clinic Dublin for conducting the gait analysis.

7. Appendix A

The softwares employed in the current work are summarised in Table 2.

8. References

[1] W. A. M. Brekelmans, H. W. Poort, and T. J. J. H. Slooff. A New Method to Analyse the Mechanical Behaviour of Skeletal Parts. *Acta Orthopaedica*, 43(5):301–317, 1972.

[2] M. Dalstra, R. Huiskes, and L. van Erning. Development and validation of a three-dimensional finite element model of the pelvic bone. *Journal of Biomechanical Engineering*, 117:272–8, 1995.

Phase of Model Development	Software/Utility	Description
CT/MRI segmentation	3DSlicer [46]	Open-source image segmentation and surface generation software
Surface processing	Meshlab [49]	Open-source software for general surface processing
Surface processing	Metro [50]	Open-source software alloying verification of decimated surfaces
Volumetric meshing	ANSYS ICEM CFD [54]	Commercial meshing software for generation of volumetric meshes
Volumetric meshing	`OpenFOAM/fluent3DMeshToFoam` [41, 42]	OpenFOAM utility to convert mesh to OpenFOAM format
Volumetric meshing	`OpenFOAM/extrudeMesh` [41, 42]	OpenFOAM utility to create cartilage volumetric mesh
Gait analysis	`OpenFOAM/visualiseGaitData` [43]	Custom OpenFOAM utility to convert gait data into a form suitable for viewing
Gait analysis	`OpenFOAM/rotateRigidFemur` [36]	Custom OpenFOAM utility for relative positioning of the femur using gait data
Solving	`OpenFOAM/elasticContactNonLinULSolidFoam` [59]	Custom OpenFOAM application for numerical calculation of displacements, stresses and strains by Finite Volume Method
Post-processing	ParaView [58]	Open-source visualisation software for post processing results

Table 2: Softwares Employed in the Current Work

[3] A. E. Anderson, C. L. Peters, B. D. Tuttle, and J. A. Weiss. Subject-specific finite element model of the pelvis: Development, validation and sensitivity studies. *Journal of Biomechanical Engineering*, 127:364–373, 2005.

[4] A. E. Anderson, B. J. Ellis, S. A. Maas, and J. A. Weiss. Effects of idealized joint geometry on finite element predictions of cartilage contact stresses in the hip. *Journal of Biomechanics*, 43:1351–7, 2010.

[5] F. Bachtar, X. Chen, and T. Hisada. Finite element contact analysis of the hip joint. *Medical & Biological Engineering & Computing*, 44: 643–51, 2006.

[6] S. Majumder, A. Roychowdhury, and S. Pal. Variations of stress in pelvic bone during normal walking, considering all active muscles. *Trends Biomater. Artif. Organs.*, 17(2):48–53, 2004.

[7] C. Silvestri. *Development and validation of a knee-thigh-hip LSDYNA model of a 50th precentile male.* PhD thesis, Worcester Polytechnic Institute, 2008.

[8] A. E. Anderson, B. J. Ellis, S. A. Maas, C. L. Peters, and J. A. Weiss. Validation of finite element predictions of cartilage contact pressure in the human hip joint. *Journal of Biomechanical Engineering*, 130:051008, 2008.

[9] A. E. Anderson, B. J. Ellis, C. L. Peters, and J. A. Weiss. Cartilage thickness: factors influencing multidetector ct measurements in a phantom study. *Radiology*, 246(1):133–141, 2008.

[10] T. Ota, I. Yamamoto, and R. Morita. Fracture simulation of the femoral bone using the finite-element method: how a fracture initiates and proceeds. *Journal of Bone and Mineral Metabolisms*, 17(2):108–112, 1999.

[11] Z. Yosibash, R. Padan, L. Joskowicz, and C. Milgrom. A ct-based high-order finite element analysis of the human proximal femur compared to in-vitro experiments. *Journal of Biomechanical Engineering*, 129(3): 297–309, 2007.

[12] F. Taddei, S. Martelli, B. Reggiani, L. Cristofolini, and M. Viceconti. Finite-element modeling of bones from CT data: sensitivity to geometry and material uncertainties. *IEEE Transactions on Bio-medical Engineering*, 53(11):2194–2200, 2006.

[13] E. S. Orwoll, L. M. Marshall, C. M. Nielson, S. R. Cummings, J. Lapidus, J. A. Cauley, K. Ensrud, N. Lane, P. R. Hoffmann, D. L. Kopperdahl, and T. M. Keaveny. Finite element analysis of the proximal femur and hip fracture risk in older men. *Journal of Bone and Mineral Research*, 24(3), 2009.

[14] M. D. Harris, A. E. Anderson, C. R. Henak, B. J. Ellis, C. L. Peters, and J. A. Weiss. Finite element prediction of cartilage contact stresses in normal human hips. *Journal of Orthopaedic Research: Official Publication of the Orthopaedic Research Society*, pages 1133–1139, 2011.

[15] H. Oonishi, H. Isha, and T. Hasegawa. Mechanical analysis of the human pelvis and its application to the artificial hip joint–by means of the three

dimensional finite element method. *Journal of Biomechanics*, 16:427–44, 1983.

[16] T. D. Brown and A. M. DiGioia. A contact-coupled finite element analysis of the natural adult hip. *Journal of Biomechanics*, 17:437–48, 1984.

[17] N .Y. P. Afoke, P. D. Byers, and W. C. Hutton. Contact pressures in the human hip joint. *The Journal of Bone & Joint Surgery*, pages 536–541, 1987.

[18] M. Dalstra and R. Huiskes. Load transfer across the pelvic bone. *Journal of Biomechanics*, 28(6):715–24, 1995.

[19] M. E. Russell, K. H. Shivanna, N. M. Grosland, and D. R. Pedersen. Cartilage contact pressure elevations in dysplastic hips: a chronic overload model. *Journal of Orthopaedic Surgery and Research*, 1:6, 2006.

[20] K. H. Shivanna, N. M. Grosland, M. E. Russell, and D. R. Pedersen. Diarthrodial joint contact models: finite element model development of the human hip. *Engineering with Computers*, 24:155–163, 2008.

[21] I. Demirdžić, D. Martinović, and A. Ivanković. Numerical simulation of thermal deformation in welded workpiece (in croatian). *Zavarivanje*, 31: 209–219, 1988.

[22] A. Ivanković, A. Muzaferija, and I. Demirdžić. Finite volume method and multigrid acceleration in modelling of rapid crack propagation in full-scale pipe test. *Computational Mechanics*, 20(1-2):46–52, 1997.

[23] I. Georgiou, A. Ivanković, A.J. Kinloch, and V. Tropsa. Rate dependent fracture behaviour of adhesively bonded joints. In A. Pavan B.R.K. Blackman and J.G. Williams, editors, *Fracture of Polymers, Composites and Adhesives II*, volume 32 of *European Structural Integrity Society*, pages 317 – 328. Elsevier, 2003.

[24] A. Karač, B.R.K. Blackman, V. Cooper, A.J. Kinloch, S. Rodriguez Sanchez, W.S. Teo, and A. Ivanković. Modelling the fracture behaviour of adhesively-bonded joints as a function of test rate. *Engineering Fracture Mechanics*, 78:973–989, 2011.

[25] I. Demirdžić and S. Muzaferija. Numerical method for coupled fluid flow, heat transfer and stress analysis using unstructured moving meshes with cells of arbitrary topology. *Computer Methods in Applied Mechanics and Engineering*, 125(1-4):235–255, 1995.

[26] H. Jasak and H. G. Weller. Application of the finite volume method and unstructured meshes to linear elasticity. *International Journal for Numerical Methods in Engineering*, pages 267–287, 2000.

[27] Y. D. Fryer, C. Bailey, M. Cross, and C. H. Lai. A control volume procedure for solving elastic stress-strain equations on an unstructured mesh. *Applied Mathematical Modelling*, 15(11-12):639–645, 1991.

[28] M. A. Wheel. A geometrically versatile finite volume formulation for plane elastostatic stress analysis. *The Journal of Strain Analysis for Engineering Design*, 31(2):111–116, 1996.

[29] Ž. Tuković, A. Ivanković, A. Karač. Finite volume stress analysis in multi-material linear elastic body. *International Journal for Numerical Methods in Engineering*, 93(4):400–419, 2012.

[30] I. Demirdžić and D. Martinović. Finite volume method for thermo-elasto-plastic stress analysis. *Computer Methods in Applied Mechanics and Engineering*, 109:331–349, 1993.

[31] I. Demirdžić, E. Džafarović, and A. I. Ivanković. Finite-volume approach to thermoviscoelasticity. *Numerical Heat Transfer, Part B: Fundamentals*, 47(3):213–237, 2005.

[32] I. Bijelonja, I. Demirdžić, and S. Muzaferija. A finite volume method for large strain analysis of incompressible hyperelastic materials. *International Journal for Numerical Methods in Engineering*, 64(12):1594–1609, 2005.

[33] P. Cardiff, A. Karač, and A. Ivanković. Development of a finite volume contact solver based on the penalty method. *Computational Material Science*, 64:283 – 284, 2012.

[34] V. Tropsa, I. Georgiou, A. Ivankovic, A. J. Kinloch, and J. G. Williams. OpenFOAM in non-linear stress analysis: Modelling of adhesive joints. In *1^{st} OpenFOAM Workshop*, Zagreb, Croatia, 2006.

[35] H. Jasak and H. Weller. Finite Volume Methodology for Contact Problems of Linear Elastic Solids. In *Proceedings of 3^{rd} International Conference of Croatian Society of Mechanics*, pages 253–260, Cavtat/-Dubrovnik, Crotatia, 2000.

[36] P. Cardiff. *Development of the Finite Volume Method for Hip Joint Stress Analysis*. PhD thesis, University College Dublin, 2012.

[37] A. Karač and Ivanković. Investigating the behaviour of fluid-filled polyethylene containers under base drop impact: A combined experimental/numerical approach. *International Journal of Impact Engineering*, 36(4):621–631, 2009.

[38] V. Kanyanta, A. Ivanković, and A. Karač. Validation of a fluid-structure interaction numerical model for predicting flow transients in arteries. *Journal of Biomechanics*, 42(11):1705–1712, 2009.

[39] A. Kelly and M. J. O'Rourke. Two system, single analysis, fluid-structure interaction modelling of the abdominal aortic aneurysms. *Proceedings of the Institution of Mechanical Engineers Part H - Journal of Engineering in Medicine*, 224(H8):955–970, 2010.

[40] H. G. Weller, G. Tabor, H. Jasak, and C. Fureby. A tensorial approach to computational continuum mechanics using object orientated techniques. *Computers in Physics*, 12(6):620–631, 1998.

[41] The OpenFOAM Extend Project. `http://www.extend-project.de`, 2012.

[42] The OpenFOAM Foundation. `http://www.openfoam.org`, 2012.

[43] P. Cardiff, A. Karač, R. Flavin, D. FitzPatrick, and A. Ivanković. Modelling the muscles for hip joint stress analysis using a finite volume methodology. In *18th Bioengineering In Ireland*, Belfast, Northern Ireland, 2012.

[44] G. Bergmann, G. Deuretzbacher, M. Heller, F. Graichen, A. Rohlmann, J. Strauss, and G. N. Duda. Hip contact forces and gait patterns from routine activities. *Journal of Biomechanics*, 34:859–71, 2001.

[45] G.E. Healthcare. `http://www.gehealthcare.com`, 2012.

[46] S. Pieper, B. Lorensen, W. Schroeder, and R. Kikinis. The NA-MIC Kit: ITK, VTK, Pipelines, Grids and 3D Slicer as an Open Platform for the Medical Image Computing Community. In *Proceedings of the 3^{rd} IEEE International Symposium on Biomedical Imaging: From Nano to Macro*, volume 1, pages 698–701, 2006.

[47] C.E. Misch. *Contemporary Implant Dentistry.* Mosby Elsevier, 3^{rd} edition, 2008.

[48] J. Vollmer, R. Mencl, and H. Muller. Improved laplacian smoothing of noisy surface meshes. *Eurographics*, 18(3):131–138, 1999.

[49] Meshlab. `http://meshlab.sourceforge.net`, 2012.

[50] P. Cignoni, C. Rocchini, and R. Scopigno. Metro: measuring error on simplified surfaces. *Computer Graphics Forum*, 17(2):167–174, 1998.

[51] M. Campen, L. Kobbelt, and M. Attene. A practical guide to polygon mesh repairing. In *Eurographics 33^{rd} Annual Conference of the European Association for Computer Graphics*, Cagliari, Sardinia, France, 2012.

[52] A. O. Cifuentes and A. Kalbag. A performance study of tetrahedral and hexahedral elements in 3-D finite element structural analysis. *Finite Elements in Analysis and Design*, 12:313–8, 1992.

[53] A. Ramos and J.A. Simoes. Tetrahedral versus hexahedral finite elements in numerical modeling of the proximal femur. *Medical Engineering & Physics*, 28:916–924, 2006.

[54] ANSYS Inc. ANSYS ICEM CFD 13.0 user manual. `http://www.ansys.com/Products/Other+Products/ANSYS+ICEM+CFD`, 2011.

[55] Charnwood Dynamics Ltd. `http://www.codamotion.com`, 2011.

[56] Central Remedial Clinic. Gait analysis at the gait lab. `http://www.crc.ie`, 2011.

[57] Kitware Inc. and VTK. VTK File Formats: The VTK User's Guide. `www.kitware.com`, 2012.

[58] Kitware Inc. and Paraview. ParaView User's Guide. `http://www.paraview.org`, 2012.

[59] P. Cardiff, A. Karač, Ž. Tuković, and A. Ivanković. Development of a finite volume based structural solver for large rotation of non-orthogonal meshes. In *7th OpenFOAM Workshop*, Darmstadt, Germany, 2012.

[60] V. K. Goel, S. Valliappan, and N. L. Svensson. Stresses in the normal pelvis. *Computers in Biology and Medicine*, 8:91–104, 1978.

[61] M. Dalstra, R. Huiskes, A. Odgaard, and L. Van Erning. Mechanical and textural properties of pelvic trabecular bone. *Journal of Biomechanics*, 26(4-5):523–535, 1993.

[62] I. Jonkers, N. Sauwen, G. Lenaerts, M. Mulier, G. Van Der Perre, and S. Jaecques. Relation between subject-specific hip joint loading, stress distribution in the proximal femur and bone mineral density changes after total hip replacement. *Journal of Biomechanics*, 41:3405–13, 2008.

[63] A. Pustoc'h and L. Cheze. Normal and osteoarthritic hip joint mechanical behaviour: a comparison study. *Medical & Biological Engineering & Computing*, 47(4):375–83, 2009.

[64] M. Taylor, K. E. Tanner, M. A. R. Freeman, and A. L. Yettram. Cancellous bone stresses surrounding the femoral component of a hip prosthesis: an elastic-plastic finite element analysis. *Med. Eng. Phys.*, 17(7): 544–550, 1995.

[65] W. Mesfar and A. Shirazi-Adl. Biomechanics of the knee joint in flexion under various quadriceps forces. *The Knee*, 12:424–434, 2005.

[66] S. Muzaferija. *Adaptive Finite Volume Method Flow Prediction Using Unstructured Meshes and Multigrid Approach.* British Thesis Service. University of London, 1994.

[67] W. A. Hodge, R. S. Fijan, K. L. Carlson, R. G. Burgess, W. H. Harris, and R. W. Mann. Contact pressures in the human hip joint measured in vivo. *Proceedings of the National Academy of Sciences of the United States of America*, 83(9), May 1986.

[68] A. T. M. Phillips, P. Pankaj, C. R. Howie, A. S. Usmani, and A. H. R. W. Simpson. Finite element modelling of the pelvis: inclusion of muscular

and ligamentous boundary conditions. *Medical Engineering & Physics*, 29(7), 739–748, 2007.

[69] J. Wolff. *The Law of Bone Remodeling (translation of the German 1892 edition)*. Springer, Berlin Heidelberg New York, 1986.